RESEARCH ARTICLE

Bithalamic gliomas may be molecularly distinct from their unilateral high-grade counterparts

Alberto Broniscer[1,2], Scott N. Hwang[3], Omar Chamdine[1], Tong Lin[4], Stanley Pounds[4], Arzu Onar-Thomas[4], Lei Chi[4], Sheila Shurtleff[5], Sariah Allen[5], Amar Gajjar[1,2], Paul Northcott[6], Brent A. Orr[5]

[1] Department of Oncology, St. Jude Children's Research Hospital, Memphis, TN.
[2] Department of Pediatrics, University of Tennessee Health Science Center, Memphis, TN.
[3] Department of Diagnostic Imaging, St. Jude Children's Research Hospital, Memphis, TN.
[4] Department of Biostatistics, St. Jude Children's Research Hospital, Memphis, TN.
[5] Department of Pathology, St. Jude Children's Research Hospital, Memphis, TN.
[6] Department of Developmental Neurobiology, St. Jude Children's Research Hospital, Memphis, TN.

Abstract

Bithalamic gliomas are rare cancers diagnosed based on poorly defined radiologic criteria. Infiltrative astrocytomas account for most cases. While some previous studies reported dismal outcomes for patients with bithalamic gliomas irrespective of therapy and histologic grade, others described better prognoses even without anticancer therapy. Little is known about their molecular characteristics. We reviewed clinical, radiologic, and histologic features of patients with bithalamic gliomas treated at our institution over 15 years. Targeted sequencing of mutational hotspots in *H3F3A*, *HIST1H3B*, *IDH1/2*, and *BRAF*, and genome-wide analysis of DNA methylation and copy number abnormalities was performed in available tumors. Eleven patients with bithalamic gliomas were identified. Their median age at diagnosis was 4.8 years (range: 1–15.7). Additional involvement of the brainstem, basal ganglia, and cerebral lobes occurred in 11, 9, and 3 cases, respectively. All patients presented with hydrocephalus. Two-thirds of the patients had a histologic diagnosis of anaplastic astrocytoma. Despite aggressive therapy, our youngest patient, the only one diagnosed before 1 year of age, is the sole long-term survivor. DNA methylation could be performed in seven tumors, all of which clustered with the RTK I 'PDGFRA' subgroup by unsupervised hierarchical analysis of methylation array against a previously published cohort of 59 pediatric high-grade gliomas. Sequencing of hotspots mutations could be done in 10 tumors, none of which harbored *H3F3A* p.K27 and/or the respective DNA methylation signature, and any other hotspot mutations. Amplification of *MDM4* (n = 2), *PDGFRA* (n = 2), and *ID2* combined with *MYCN* (n = 1) were observed in 7 tumors available for analysis. In comparison with the previously published experience with unilateral high-grade thalamic astrocytomas where *H3F3A* p.K27 was present in two-thirds of cases, the absence of this molecular subgroup in bithalamic gliomas was striking. This finding suggests that unilateral and bithalamic high-grade gliomas may represent two distinct molecular entities.

INTRODUCTION

Thalamic tumors account for approximately 5% of all central nervous system (CNS) cancers in children and consist mostly of astrocytomas with unilateral involvement (4, 17, 19, 23). Bithalamic gliomas represent a rare subset of poorly understood tumors diagnosed based on symmetrical involvement of both thalami (5, 7, 8, 14, 17, 19, 23). Although histologic confirmation is warranted for the diagnosis of bithalamic gliomas since their imaging characteristics overlap with those of other oncologic and non-oncologic entities, (13) some studies have included patients with only radiologic diagnosis (5, 14, 23). Infiltrative low- and high-grade astrocytomas account for most bithalamic gliomas (5, 8, 14, 17, 19, 23). The treatment and prognosis of patients with bithalamic gliomas remains controversial (5, 8, 14, 17, 19, 23). While some studies reported a dismal outcome for patients with bithalamic gliomas irrespective of therapy and histologic grade, (8, 19) others have reported long-term survivors, including patients who underwent only tumor biopsy and/or decompression of hydrocephalus (5, 14, 17, 23).

Very little is known about the molecular characteristics of bithalamic gliomas since suitable tissue for detailed analysis is rarely

Table 1. Clinical, radiologic, and histologic characteristics of all patients.

Patient no.	Age at diagnosis (yrs)/gender	Interval between onset of symptoms and diagnosis (days)	Race/ethnicity	No. of gray matter areas affected	Histologic diagnosis/surgery	Therapy	Survival (yrs)
1	1.0/F	120	Caucasian	3	AA/biopsy	Chemotherapy	7.2 +
2	2.4/M	14	Caucasian	3	Glioblastoma/STR	Chemotherapy	0.5
3	2.4/M	21	Caucasian	5	AA/biopsy	RT + chemotherapy	0.8
4	3.3/M	1	Mixed race	4	HGG with small cell features/STR	RT + chemotherapy	1.0
5	4.3/F	60	Hispanic	6	AA/biopsy	RT + chemotherapy	0.75
6	4.8/M	5	African-American	6	GBM/STR	RT + chemotherapy	1.0
7	5.4/M	7	Caucasian	6	AA/biopsy	RT + chemotherapy	1.2
8	9.8/F	35	Caucasian	7	AA/biopsy	RT + chemotherapy	1.5
9	10.7/M	30	Caucasian	6	AA/biopsy	RT + chemotherapy	1.2
10	14.9/F	42	African-American	7	Diffuse astrocytoma WHO grade II/biopsy	RT + chemotherapy	1.75
11	15.7/F	30	Caucasian	5	AA/biopsy	RT + chemotherapy	1.0

Abbreviations: No. = number; yrs = years; F = female; M = male; AA = anaplastic astrocytoma; GBM = glioblastoma; HGG = high-grade glioma; WHO = World Health Organization; STR = subtotal resection; RT = radiation therapy.

obtained from small tumor biopsies (1, 27, 28). We conducted clinical, radiologic, and histologic review, and molecular analysis of a cohort of children with bithalamic gliomas. Unlike unilateral high-grade thalamic astrocytomas, (11, 21, 25, 30) bithalamic gliomas lacked *H3F3A* p.K27M mutation and/or the respective DNA methylation characteristics, which suggests that both represent separate molecular entities.

MATERIALS AND METHODS

Following institutional review board approval, we retrospectively reviewed the clinical and radiologic characteristics of all patients younger than 22 years with newly diagnosed bithalamic gliomas treated at our institution from March 1999 until August 1, 2014.

We defined bithalamic gliomas as tumors arising bilaterally and completely involving both thalami. Cases with a predominant unilateral involvement and partial spread to the contralateral side and those who developed a bithalamic appearance only at the time of progression were excluded from this analysis. Only patients with diffusely infiltrating gliomas were included in this study and the histologic diagnosis of pilocytic astrocytoma was an exclusion criterion.

Detailed clinical and therapy-related data were collected for all patients. Brain MRIs at diagnosis of suspected cases were selected by a neuro-oncologist (AB) and then independently reviewed by a neuro-radiologist (SNH). A scoring system was used to assess the extent of gray matter involvement by T_2-weighted and/or FLAIR MRI sequences in the thalami, deep-seated structures (ie, lentiform nucleus, caudate nucleus, insula, brainstem, and cerebellum), and cerebral lobes as previously described (6). A score of 1 was attributed to involvement of each unilateral structure, the brainstem, and cerebellum. Assessment of the presence of tumor mass was based on T_1- and T_2-weighted/FLAIR signal characteristics independent of the presence of contrast enhancement. All cases underwent histologic review by a board-certified neuro-pathologist (BAO) according to the 2016 World Health Organization (WHO) classification. Immunoreactivity of H3K27M was tested on 4-μm formalin fixed

paraffin-embedded (FFPE) sections as previously described using a polyclonal antibody (Millipore Sigma, Darmstadt, Germany, catalog number ABE419, 1:400) (28). Immunohistochemistry of p53 (Zeta Corporation Arcadia, CA, USA, clone DO-7, 1:200), ATRX (Sigma, catalog number HPA001906, 1:600), and H3K27me3 (Cell Signaling Technology, Denver, MA, USA, C36B11, 1:200) were performed according to the manufacturer's specifications.

Molecular studies

Dual-color fluorescence in situ hybridization (FISH) was performed on 4-μm formalin-FFPE tissue sections. Break-apart and fusion probes for *FGFR1* were derived from BAC clones RP11-246A12 and RP11-118H9 (BACPAC Resources, Oakland, CA). Probes were labeled with either AlexaFluor-488 or AlexaFluor-555 fluorochromes and nuclei were counterstained with DAPI (200 ng/mL; Vector Laboratories Inc., Burlingame, CA) for viewing on an Olympus BX51 fluorescence microscope equipped with a 100-W mercury lamp; FITC, Rhodamine, and DAPI filters; 100X PlanApo (1.40) oil objective; and a Jai CV digital camera. Images were captured and processed using the Cytovision v7.3 software (Leica Biosystems, Inc., Buffalo Grove, IL, USA).

DNA was extracted from FFPE tissue using the Maxwell® 16 Plus LEV DNA purification kit (Promega, Madison, WI, USA) according to the manufacturer's instructions. DNA was quantified using the Qubit dsDNA BR assay kit (ThermoFisher Scientific, Grand Island, NY, USA).

Targeted sequencing of *BRAF* p.V600, *H3F3A* p.K27, *H3F3A* p.G34, *HIST1H3B* p.K27, *IDH1* p.R132, and *IDH2* p.R172 was performed as previously described (6, 29)

Illumina infinium human 450 k bead array

Processing and acquisition of DNA methylation data were performed as previously described (6).

Analysis of DNA methylation data was performed using the open source statistical programming language R (18). Files with

raw data generated by the iScan microarray scanner (Illumina, San Diego, CA) were read and processed using the *minfi* Bioconductor package as described in the Illumina GenomeStudio software (Illumina, San Diego, CA, USA) (2). Further filtering of the probes was done as previously described (25). In total, 438 370 probes were kept for clustering analysis. To determine the subgroup affiliation of our cohort by methylation array, we used previously published data of DNA methylation in pediatric high-grade gliomas as a reference (n = 59; GSE36278) (25). Missing values were imputed using a k-nearest neighbor algorithm (26). We selected the top 10 000 most variable methylation probes as measured by standard deviation across the combined dataset to conduct an unsupervised hierarchical clustering of bithalamic tumors and 59 reference samples. Samples were then clustered by applying the Ward's method and dissimilarity based on Euclidean distance. Methylation probes in the heatmap were reordered by hierarchical clustering using a similar approach.

We compared the methylation profile of tumors (n = 7) in the current manuscript to that of previously published unilateral thalamic high-grade gliomas (n = 8) (25). We used the minfi package to obtain normalized M-values for the methylation profile of each tumor (2). For each gene, we used Illumina annotation to identify all probes within the promoter region defined as the area within 1000 base pairs upstream of the transcription start site. For each gene and tumor, we then computed the average M-value for this promoter region. Next, for each gene promoter region, we used the Welch t-test to compare the average promoter M-values of bithalamic (n = 7) and unilateral tumors (n = 8). To address multiple-testing, we used a robust method to estimate the false discovery rate as a function of *P*-value (16). To gain further biological insight from our study, we used the multi-response permutation procedure (MRPP) to evaluate differential methylation of 9063 gene-sets defined in the molecular signatures data base (MsigDB; http://software.broadinstitute.org/gsea/msigdb/) with statistical significance determined by 10 000 permutations of group label assignments (15).

Analysis of copy number abnormalities based on the 450 k Infinium methylation array was performed by using the *conumee* Bioconductor package (12). The combined intensities of all available CpG probes were normalized against 12 control samples from normal brain tissue using a linear-regression approach. Probes were combined into genomic bins of 10 kb. Bins comprised of less than 10 probes were repeatedly merged with the adjacent bins. Subsequent analysis was performed with default setting in the *conumee* package. Detection of amplification and chromosomal gains and losses was performed by manual assessment of the respective loci for each individual profile following automatic scoring (6, 25).

A logistic regression model to estimate the probability of MGMT promoter methylation from the 450 k methylation array was performed as previously described (3).

Tumor and germline samples from one patient included in this study had already undergone whole exome sequencing as part of the Pediatric Cancer Genome Project (30).

Other statistical analyses

Descriptive statistical analyses were used to summarize the demographic and clinical characteristics of the patients. Overall survival (OS) was defined as the interval between date of diagnosis and
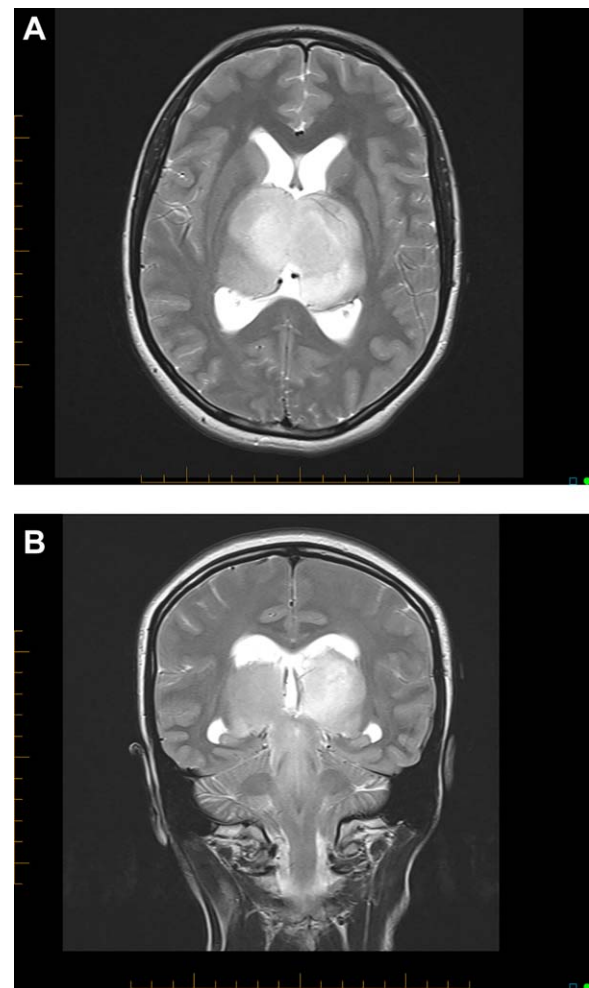

Figure 1. Axial T_2-weighted brain MRI of patient 11 showing symmetrical bithalamic involvement (**A**). This patient was also found to have hydrocephalus based on symptoms and enlargement of lateral ventricles with transependymal flow in their frontal horns. Coronal T_2-weighted brain MRI of same patient showing symmetrical bithalamic and midbrain involvement (**B**).

death. Patients who were alive were censored at the time of last contact. The Wilcoxon rank sum test was used to assess the associations between categorical variables (ie, gender, presence of tumor mass, and contrast enhancement) and continuous variables (ie, age at diagnosis, interval from onset of symptoms and diagnosis, and number of gray matter areas affected). The Kruskal–Wallis test was used to test any associations between histologic diagnosis and the same continuous variables. Cox models were used to assess for associations between OS and continuous variables and two-sided log-rank tests were used for categorical variables.

RESULTS

We identified 11 patients (5 [45%] females) with bithalamic gliomas (Table 1). The median age at diagnosis was 4.8 years (range: 1.0–15.7). Only one patient was younger than one 1 year at diagnosis. The median latency from onset of symptoms to diagnosis was
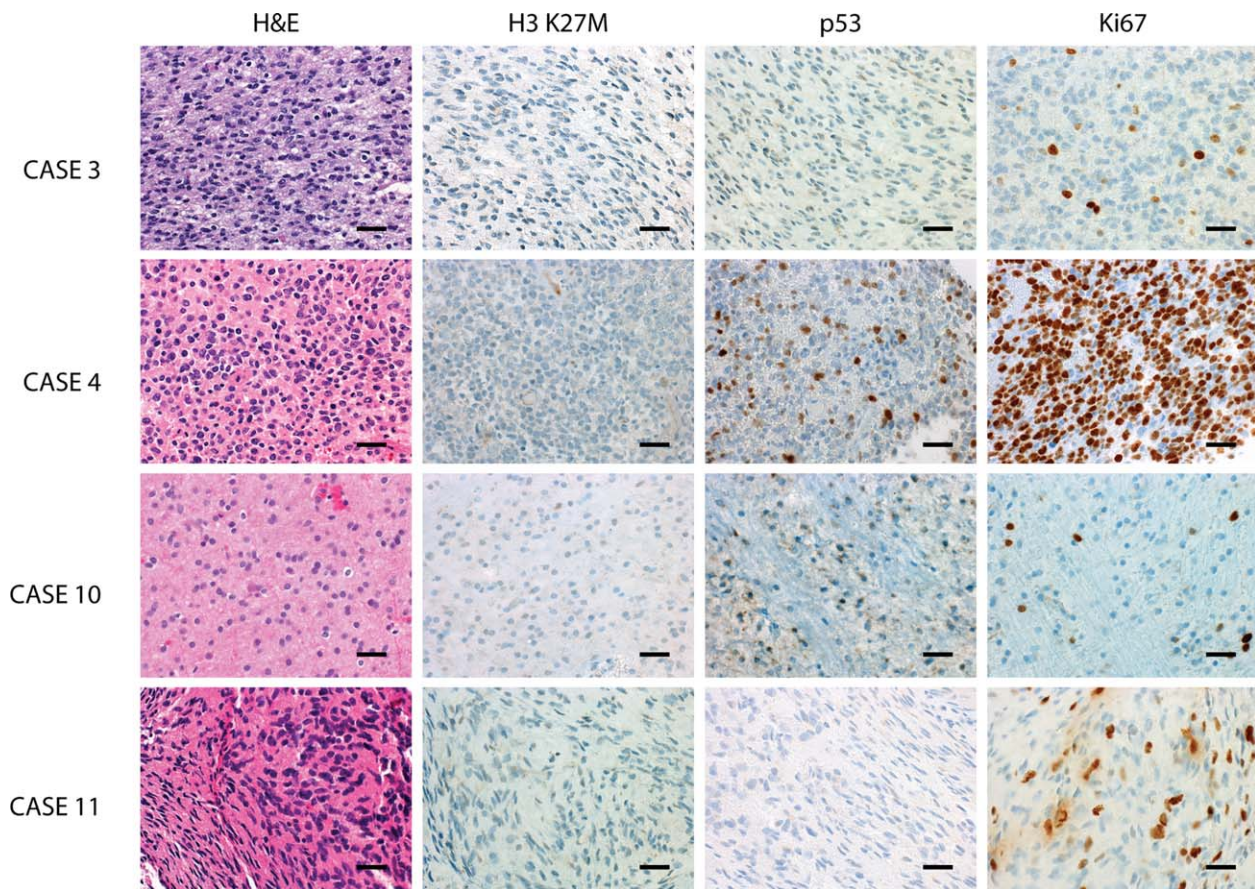
Figure 2. Representative histomorphology and immunophenotype of bithalamic gliomas demonstrating infiltrative growth and moderate cytologic pleomorphism. While tumors lacked immunoreactivity for H3K27M, p53 expression was mostly seen in a minority of tumor cells. The proliferative fraction, as assessed by Ki67/Mib-1 immunolabeling, was variable from moderately to very high frequency. The scale bars represent 200 μm.

30 days (range: 1–120 days). Patient 4 had a 24-h history precipitated by massive intra-tumoral hemorrhage. Most patients presented with signs of increased intracranial pressure. Only two patients had complaints of new pyramidal signs. None of the patients had seizures at presentation.

Figure 1A shows typical MRI characteristics observed in patient 11. All patients presented with hydrocephalus which was decompressed by placement of a ventriculo-peritoneal shunt (n = 5) or third ventriculostomy (n = 5). Patient 4 had improvement of hydrocephalus following subtotal resection of the tumor. Tumor infiltration of the brainstem and basal ganglia were observed in 11 and 9 patients, respectively (Figure 1B). Patients 8, 10, and 11 had additional involvement of 2, 1, and 2 cerebral lobes at diagnosis, respectively. Distinct tumor masses were observed within the infiltrated thalami in 5 patients, 4 of which enhanced after contrast administration. Patients had a median of 6 (range: 3–7) gray matter areas involved at diagnosis.

All patients underwent histologic confirmation (Table 1). The majority of samples analyzed consisted of at least 80% tumor cells. Two-thirds (7 of 11) of the patients had a histologic diagnosis of anaplastic astrocytoma (WHO grade III). Three patients had a glioblastoma (WHO grade IV). Only one patient had a diffuse

astrocytoma (WHO grade II; patient 10, Figure 2). All tumors consisted of infiltrative astrocytomas with round to oval nuclear morphology. The tumors lacked specific histologic findings except for one case which demonstrated a small-cell phenotype (patient 4) and another that had scattered multinucleated giant cells (patient 9). Expression of p53 by immunohistochemistry could be assessed in 6 cases, one of which (patient 5) displayed a strong and diffuse pattern suggestive of a mutant *TP53*. While ATRX protein loss was observed in one (patient 4) of 5 cases, mutant H3K27M was not detected in 5 tumors with available tissue (Figure 2). H3K27me3 demonstrated heterogeneous expression in 5 tumors tested.

Molecular studies

Unsupervised hierarchical clustering of genome-wide methylation was conducted in 7 (64%) tumors for which adequate DNA was available. By comparing with a previously published dataset of pediatric high-grade gliomas, (25) our cohort clustered with the RTK I 'PDGFRA' subgroup (Figure 3 and Table 2). A subgroup representing either *H3F3A* p.K27- or p.G34-mutated tumors was not observed. Only one tumor in the RTK I 'PDGFRA' subgroup displayed MGMT promoter methylation (Table 2).
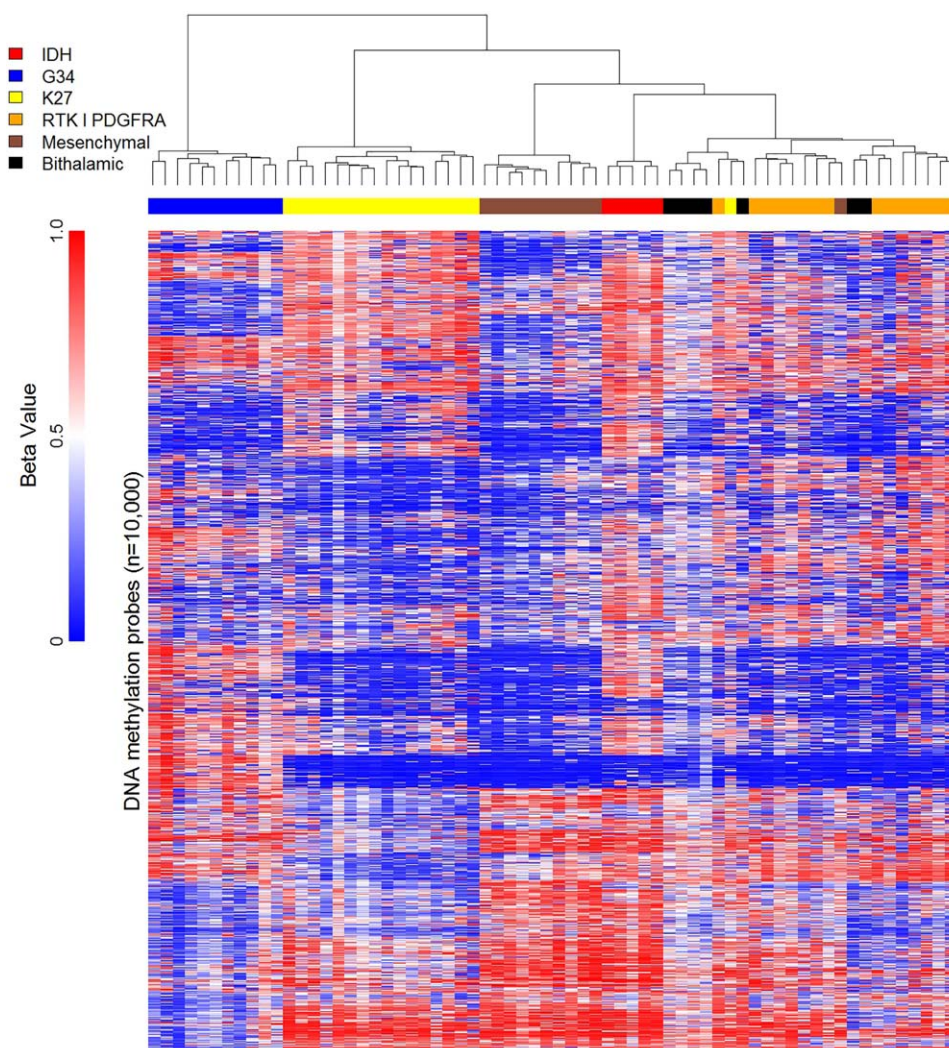
Figure 3. Heatmap representation of unsupervised hierarchical clustering analysis of 450 k methylation array profiles in 7 pediatric patients with bithalamic gliomas in comparison with a dataset of 59 previously published pediatric high-grade gliomas.

We observed 364 genes with differentially methylated promoter regions comparing unilateral and bithalamic tumors (estimated false discovery rate of 0.001) (Supporting Information Table 1). Thirty-two of these genes exhibited greater methylation in bithalamic compared with unilateral tumors. The remaining 332 genes exhibited greater methylation in unilateral tumors. The top 100 genes sets that differed between the two groups are presented in Supporting Information Table 2.

Sequencing of hotspot mutations was available in 10 (91%) patients. No mutations were observed in *H3F3A* p.K27, *H3F3A* p.G34, *HIST1H3B* p.K27, *IDH1* p.R132, *IDH2* p.R172, and *BRAF* p.V600 (Table 2). *EGFR* and *TP53* mutations were demonstrated in the tumor that had previously undergone whole exome sequencing (30) (Table 2).

Amplification of multiple oncogenes including *MDM4* (n = 2), *PDGFRA* (n = 2), *CDK6* (n = 1), *EGFR* (n = 1), and a combination of *ID2* and *MYCN* (n = 1) was observed (Table 2). *FGFR1* fusions were not detected using break-apart FISH probes in 6 tumors with sufficient material. Further confirmation of copy number abnormalities by FISH was not possible due to limited amount of leftover tumor. The most common areas of large gains in 7

tumors were chromosome 7 (71%), 1q (57%), chromosome 2 (43%), 17q (43%), and chromosome 8, 9q, 12p, 13q, and 15q in 28.5% of tumors each. Likewise, the most common areas of large chromosomal losses were 4q (43%), 17p (43%), and 11q, 14q, and 16q in 28.5% of tumors each.

Outcome

Despite aggressive treatment with chemotherapy with or without radiation therapy (RT), (Table 1) only the patient diagnosed as an infant remains alive 7.2 years after diagnosis (Figure 4). Eight patients experienced local disease progression only. Patient 7 experienced massive leptomeningeal spread in his spine following local RT. The pattern of disease progression was not documented in one case. The median OS for all patients was 1 year (range: 0.5 to 7.2 + years). In this cohort, female patients were more likely to have longer intervals from onset of symptoms to diagnosis (median 42 vs. 10.5 days; $P = 0.0065$). None of the continuous and categorical variables analyzed showed any association with each other or with OS likely due to small sample size.

Table 2. Molecular characteristics of evaluable tumors.

Patient no.	Methylation subgroup	MGMT promoter methylation	*IDH1* p.R132H	*H3F3A* p.G34	*H3F3A* p.K27	*HIST1H3B* p.K27	*CDKN2A* Loss	Other relevant molecular abnormalities
1	NA	NA	No	No	No	NA	NA	NA
3	RTK I 'PDGFRA'	Methylated	No	No	No	No	No	No
4	RTK I 'PDGFRA'	Unmethylated	No	No	No	No	No	*PDGFRA* amplification
5	RTK I 'PDGFRA'	Unmethylated	No	No	No	No	No	*PDGFRA* and *EGFR* amplification
6*	NA	NA	No	No	No	No	No	*PDGRFA* (structural variation), *EGFR* G598V (LOH) and *TP53* R175H (LOH)
7	RTK I 'PDGFRA'	Unmethylated	No	No	No	No	No	*MDM4*, *ID2*, and *MYCN* amplification
8	NA	NA	No	NA	No	NA	NA	NA
9	RTK I 'PDGFRA'	Unmethylated	No	No	No	No	No	No
10	RTK I 'PDGFRA'	Unmethylated	No	No	No	No	No	*MDM4* amplification
11	RTK I 'PDGFRA'	Unmethylated	No	No	No	No	No	*CDK6* amplification

*Patient whose tumor previously underwent whole exome sequencing.

Abbreviations: No. = number; MGMT = methylguanine methyltransferase; NA = not available; LOH = loss of heterozygosity.

DISCUSSION

We report for the first time detailed molecular characteristics of one of the largest cohorts to date of patients with bithalamic gliomas. Since this is a rare and poorly defined entity, previous studies contained a maximum of 15 affected subjects, even when reviewing the experience within entire countries (5, 8, 14, 17, 19, 23) (Table 3). The most remarkable molecular finding of our study was the complete lack of *H3F3A* p.K27 and/or the respective DNA methylation signature. The presence of *H3F3A* p.K27 and/or expression of the respective protein have been documented by sequencing or immunohistochemistry in approximately 70% of thalamic high-grade astrocytomas (1, 9, 11, 20–22, 25, 27, 28) (Table 4). To our knowledge, molecular characteristics of only a few bithalamic high-grade gliomas, one of which harbored the *H3F3A* p.K27 mutation, had been previously reported (1, 27, 28, 30). Since most

Figure 4. Axial T_2-weighted brain MRI of the only long-term survivor (patient 1) at diagnosis. A tumor biopsy was obtained from the T_2 hyperintense anterior portion of the right thalamus.

patients with bithalamic gliomas undergo at most a biopsy, their representation in molecular studies would be assumed to be exceptional. Assuming that 70% of unilateral high-grade thalamic astrocytomas harbor an *H3F3A* p. K27 mutation, (1, 9, 11, 20–22, 25, 27, 28) our results are substantially different despite the limited sample size ($P = 5.9 \times 10^{-6}$). The absence of other hotspot mutations including *H3F3A* p.G34 in our patients was not surprising because they predominantly occur in tumors arising in the cerebral cortex (21, 25, 30). In contrast to diffuse intrinsic pontine gliomas, another common pediatric midline CNS cancer, (11, 30) we did not observe hotspot *HIST1H3B* mutations in bithalamic gliomas.

Although our results showed differentially methylated genes comparing unilateral and bithalamic gliomas, (Supporting Information Tables 1 and 2) including those involved in DNA repair, cell-cycle progression, and apoptosis, no solid conclusions can be drawn from such preliminary data.

Similar to other studies, (11, 21, 25, 30) we observed multiple other amplified oncogenes (ie, *MDM4*, *MYCN*, *PDGFRA*, and *CDK6*) in our patients. One tumor (patient 7) had concurrent amplification of *MYCN* and *ID2*, a finding recently reported in a subset of supratentorial high-grade gliomas (24).

In contrast to two previous studies, (8, 14) our patients' tumors commonly infiltrated adjacent structures, including the midbrain, basal ganglia, and in a few cases even cerebral lobes. The involvement of cerebral lobes in a minority of cases was reminiscent of gliomatosis cerebri, a condition where typical bithalamic involvement was seen in one-fourth of patients (6). We confirmed that the risk of hydrocephalus is extremely high in bithalamic gliomas.

We acknowledge the bias of the current study since high-grade gliomas accounted for 90% of cases in contrast to previous reports where low-grade gliomas predominated (5, 8, 14, 17, 19). Sampling error of tiny biopsies in such extensive tumors probably accounts for some of this difference. We had already shown that even histologic low-grade bithalamic gliomas portend a dismal prognosis (19). A few previous studies included patients without histologic confirmation, some of which were long-term survivors despite not receiving any anticancer therapy (5, 14, 17, 23). We
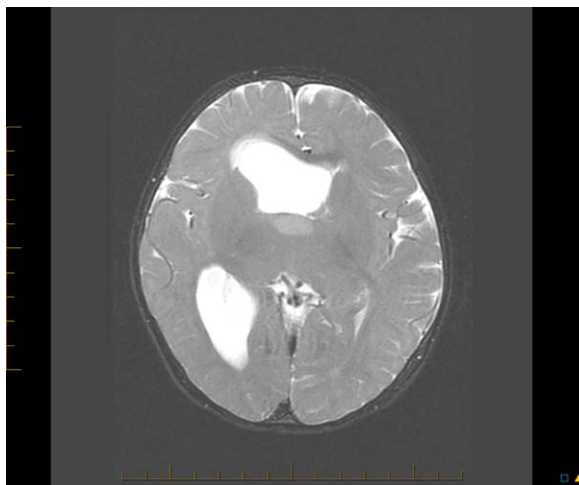
Table 3. Summary of previous series of patients with bithalamic gliomas.

Author	Year of publication	Number of patients	Median age at diagnosis/range (years)	Histologic diagnosis	Upfront therapy	Outcome
Reardon *et al*	1998	12	NA/≤ 18	LGG: 9; HGG: 3	Not specified	3-year OS = 0%
Di Rocco *et al*	2002	4	8/0.25–10	DA grade II: 3; astrocytoma grade III: 1	RT: 4	Three patients deceased with median survival of 10 months; One patient alive after 8 months
Puget *et al*	2007	9	9.6 (mean)/NA	PA: 1; LGG: 6; HGG: 2	RT: 4	Four patients deceased; Five long-term survivors received no adjuvant therapy (mean F/U of 4.5 years)
Menon *et al*	2010	7	17/5–29	DA grade II (6); NC (1)	RT: 7	All patients alive for a median F/U of 1 year (range; 1–5 years)
Steinbok *et al*	2015	10	6.6 (mean)/1.5–14.7	PA: 1; DA grade II: 3; AA: 2; GBM: 3; NC: 1	Chemotherapy: 5; RT: 3	Seven patients deceased with median survival of 11.3 months; Three long-term survivors received no adjuvant therapy
Boesten *et al*	2016	15	7.5/2–15.1	PA: 2; DA grade II: 9; LGG: 1; NC: 3	Chemotherapy: 3; RT: 3	10-year EFS: 16% ± 13%; 10-year OS: 65% ± 13%

Abbreviations: NA = not available; NC = not confirmed; LGGs = low-grade glioma; HGG = high-grade glioma; DA = diffuse astrocytoma; PA = pilocytic astrocytoma; AA = anaplastic astrocytoma; GBM = glioblastoma; RT = radiation therapy; EFS = event-free survival; OS = overall survival; F/U = follow-up.

Table 4. Summary of *H3F3A* p.K27 mutations in unilateral high-grade gliomas identified by sequencing and/or immunohistochemistry.

Study	Number of patients	Median age at diagnosis (range; years)	% Tumors harboring *H3F3A* p.K27
Schwartzentruber *et al* (2012)	6	10.5 (6–14)	50%
Sturm *et al* (2012)	8	11 (6–23)	100%
Venneti *et al* (2013)	3	11.6 (7–21.4)	100%
Aihara *et al* (2014)	18	42 (17–78)	55%
Fontebasso *et al* (2014)	11	11 (6–15)	82%
Venneti *et al* (2014)	7	12 (7–21)	71%
Feng *et al* (2015)*	15	31.7 (mean; 22–53)	66.7%
Solomon *et al* (2015)[†]	23	Adults and children	65%
Ryall *et al* (2016)	22	10.9 (4–17.6)	50%
Total	113		65%

*Four patients included had a grade II glioma.

[†]One of 15 tumors harboring an *H3F3A* p.K27 was a grade 2 glioma. Histologic grade was not provided for 8 tumors.

suspect that some of these patients with better outcomes might have a pilocytic astrocytoma. Pilocytic astrocytomas can display an infiltrative aspect with bithalamic involvement. When patients with thalamic gliomas undergo small biopsies, commonly the only means to differentiate tumors with better or worse prognosis is the presence of suggestive molecular features (eg, *BRAF* fusion) (10, 20). We removed patients with pilocytic astrocytomas from the current analysis because they represent a separate entity with a potentially better prognosis. Since the radiologic characteristics of bithalamic gliomas overlap with other oncologic and non-oncologic entities, (13) we strongly recommend histologic confirmation before these patients are considered for any anticancer therapy.

The confusion in the definition of bithalamic gliomas accounts for the controversy in therapeutic approaches and outcomes reported for affected patients. While some studies described a terrible outcome for most patients despite treatment with RT with or without chemotherapy, (8, 19, 23) others reported several long-term survivors (5, 14, 17, 23). Unfortunately, conventional methods may not be sufficient to distinguish bithalamic gliomas in clinical practice. The absence of immunoreactivity can rule out *H3F3A* p.K27 mutant diffuse midline gliomas. However, the heterogeneous immunolabeling of H3K27me3 stains was not useful in our diagnostic work-up.

Until the imaging, histologic, and molecular characteristics of bithalamic gliomas are clearly defined, no consensus will emerge about their natural history, best therapeutic approaches, and prognosis of affected patients.

One of the limitations of this study was our inability to perform additional confirmatory or other exploratory molecular analyses caused by the lack of further tissue for analysis.

One previous study had speculated that bithalamic gliomas constitute a separate entity based on their unique clinical and radiologic characteristics (8). Although the number of tumors analyzed was

limited, the complete absence of *H3F3A* p.K27-mutated tumors among our patients is in stark contrast to other thalamic high-grade gliomas. Therefore, our results suggest that bithalamic gliomas may represent a distinct entity compared with unilateral thalamic high-grade gliomas.

ACKNOWLEDGMENTS

CONFLICT OF INTEREST

The authors have no conflicts of interest to disclose related to this manuscript.

REFERENCES

1. Aihara K, Mukasa A, Gotoh K, Saito K, Nagae G, Tsuji S *et al* (2014) H3F3A K27M mutations in thalamic gliomas from young adult patients. *Neuro Oncol* **16**:140—146.
2. Aryee MJ, Jaffe AE, Corrada-Bravo H, Ladd-Acosta C, Feinberg AP, Hansen KD, Irizarry RA (2014) Minfi: a flexible and comprehensive Bioconductor package for the analysis of Infinium DNA methylation microarrays. *Bioinformatics* **30**:1363—1369.
3. Bady P, Sciuscio D, Diserens AC, Bloch J, van den Bent MJ, Marosi C *et al* (2012) MGMT methylation analysis of glioblastoma on the Infinium methylation BeadChip identifies two distinct CpG regions associated with gene silencing and outcome, yielding a prediction model for comparisons across datasets, tumor grades, and CIMP-status. *Acta Neuropathol* **124**:547—560.
4. Bilginer B, Narin F, Işıkay I, Oguz KK, Söylemezoglu F, Akalan N (2014) Thalamic tumors in children. *Childs Nerv Syst* **30**:1493—1498.
5. Boesten T, Gerber NU, Kandels D, Azizi AA, Schmidt R, Warmuth-Metz M *et al* (2016) Management of primary thalamic low-grade glioma in pediatric patients: results of the multicenter treatment studies HIT-LGG 1996 and SIOP-LGG 2004. *Neuro Oncol Pract* doi: 10.1093/nop/npw007 (in press).
6. Broniscer A, Chamdine O, Hwang S, Lin T, Pounds S, Onar-Thomas A *et al* (2016) Gliomatosis cerebri in children shares molecular characteristics with other pediatric gliomas. *Acta Neuropathol* **131**:299—307.
7. Colosimo C, di Lella GM, Tartaglione T, Riccardi R (2002) Neuroimaging of thalamic tumors in children. *Childs Nerv Syst* **18**:426—439.
8. Di Rocco C Iannelli A (2002) Bilateral thalamic tumors in children. *Childs Nerv Syst* **18**:440—444.
9. Feng J, Hao S, Pan C, Wang Y, Wu Z, Zhang J *et al* (2015) The H3.3 K27M mutation results in a poorer prognosis in brainstem gliomas than thalamic gliomas in adults. *Human Pathol* **46**:1626—1632.
10. Fontebasso AM, Bechet D, Jabado N (2013) Molecular biomarkers in pediatric glial tumors: a needed wind of change. *Curr Opin Oncol* **25**:665—673.
11. Fontebasso AM, Papillon-Cavanagh S, Schwartzentruber J, Nikbakht H, Gerges N, Fiset PO *et al* (2014) Recurrent somatic mutations in

12. ACVR1 in pediatric midline high-grade astrocytoma. *Nat Genet* **46**:462—466.
13. Hovestadt V, Zapatka M *conumee*: Enhanced copy-number variation analysis using Illumina 450k methylation arrays. R package version 0.99.4. In: *Bioconductor: Open Source Software for Bioinformatics*. http://www.bioconductor.org/packages/release/bioc/html/conumee.html.
14. Khanna PC, Iyer RS, Chaturvedi A, Thapa MM, Chaturvedi A, Ishak GE, Shaw DW (2011) Imaging bithalamic pathology in the pediatric brain: demystifying a diagnostic conundrum. *Am J Roentgenol* **197**:1449—1459.
15. Menon G, Nair S, Sudhir J, Rao BR, Krishnakumar K (2010) Bilateral thalamic lesions. *Br J Neurosurg* **24**:566—571.
16. Nettleton D, Recknor J, Reecy JM (2008) Identification of differentially expressed gene categories in microarray studies suing nonparametric multivariate analysis. *Bioinformatics* **24**:192—201.
17. Pounds S, Cheng C (2006) Robust estimation of the false discovery rate. *Bioinformatics* **22**:1979—1987.
18. Puget S, Crimmins DW, Garnett MR, Grill J, Oliveira R, Boddaert N *et al* (2007) Thalamic tumors in children: a reappraisal. *J Neurosurg* **106**:354—362.
19. R Core Team (2015). *R: A Language and Environment for Statistical Computing*, R Foundation for Statistical Computing: Vienna, Austria. https://www.R-project.org/
20. Reardon DA, Gajjar A, Sanford RA, Heideman RL, Walter AW, Thompson SJ *et al* (1998) Bithalamic involvement predicts poor outcome among children with thalamic glial tumors. *Pediatr Neurosurg* **29**:29–35.
21. Ryall S, Krishnarty R, Arnoldo A, Buczkowicz P, Mistry M, Siddaway R *et al* (2016) Targeted detection of genetic alterations reveal the prognostic impact of H3K27M and MAPK pathway aberrations in paediatric thalamic glioma. *Acta Neuropathol Commun* **4**:93—103.
22. Schwartzentruber J, Korshunov A, Liu XY, Jones DT, Pfaff E, Jacob K *et al* (2012) Driver mutations in histone H3.3 and chromatin remodelling genes in paediatric glioblastoma. *Nature* **482**:226—231.
23. Solomon DA, Wood MD, Tihan T, Bollen AW, Gupta N, Phillips JJ, Perry A (2015) Diffuse midline gliomas with histone H3-K27M mutation: a series of 47 cases assessing the spectrum of morphologic variation and associated genetic alterations. *Brain Pathol* **26**:569—580.
24. Steinbok P, Gopalakrishnan CV, Hengel AR, Vitali AM, Poskitt K, Hawkins C *et al* (2015) Pediatric thalamic tumors in the MRI era: a Canadian perspective. *Childs Nerv Syst* **32**:269—280.
25. Sturm D, Orr BA, Toprak UH, Hovestadt V, Jones DT, Capper D *et al* (2016) New brain tumor entities emerge from molecular classification of CNS-PNETs. *Cell* **164**:1060—1072.
26. Sturm D, Witt H, Hovestadt V, Khuong-Quang DA, Jones DT, Konermann C *et al* (2012) Hotspot mutations in H3F3A and IDH1 define distinct epigenetic and biological subgroups of glioblastoma. *Cancer Cell* **22**:425—437.
27. Troyanskaya O, Cantor M, Sherlock G, Brown P, Hastie T, Tibshirani R *et al* (2001) Missing value estimation methods for DNA microarrays. *Bioinformatics* **17**:520—525.
28. Venneti S, Garimella MT, Sullivan LM, Martinez D, Huse JT, Heguy A *et al* (2013) Evaluation of histone 3 lysine 27 trimethylation (H3K27me3) and enhancer of Zest 2 (EZH2) in pediatric glial and glioneuronal tumors shows decreased H3K27me3 in H3F3A K27M mutant glioblastomas. *Brain Pathol* **23**:558—564.
29. Venneti S, Santi M, Felicella MM, Yarilin D, Phillips JJ, Sullivan LM *et al* (2014) A sensitive and specific histopathologic prognostic marker for H3F3A K27M mutant pediatric glioblastomas. *Acta Neuropathol* **128**:743—753.
30. Wu G, Broniscer A, McEachron TA, Lu C, Paugh BS, Becksfort J *et al* (2012) Somatic histone H3 alterations in pediatric diffuse intrinsic pontine gliomas and non-brainstem glioblastomas. *Nat Genet* **44**:251–253.

30. Wu G, Diaz AK, Paugh BS, Rankin SL, Ju B, Li Y *et al* (2014) The genomic landscape of diffuse intrinsic pontine glioma and pediatric non-brainstem high-grade glioma. *Nat Genet* **46**: 444–450.

SUPPORTING INFORMATION

Additional Supporting Information may be found in the online version of this article at the publisher's web-site:

Table S1. List of 364 genes with differentially methylated promoter regions comparing unilateral and bithalamic gliomas. Beta values ranged from 0 (no methylation) to 1 (complete methylation). FDR stands for false discovery rate.

Table S2. List of 100 gene sets with strongest differential methylation.